

# YOLO-based Bearing Fault Diagnosis With Continuous Wavelet Transform

Po-Heng Chou, *Member, IEEE*, Wei-Lung Mao, and Ru-Ping Lin

**Abstract**—This letter proposes a YOLO-based framework for spatial bearing fault diagnosis using time–frequency spectrograms derived from continuous wavelet transform (CWT). One-dimensional vibration signals are first transformed into time–frequency spectrograms using Morlet wavelets to capture transient fault signatures. These spectrograms are then processed by YOLOv9, v10, and v11 models to classify fault types. Evaluated on three benchmark datasets, including Case Western Reserve University (CWRU), Paderborn University (PU), and Intelligent Maintenance System (IMS), the proposed CWT–YOLO pipeline achieves significantly higher accuracy and generalizability than the baseline MCNN–LSTM model. Notably, YOLOv11 reaches mAP scores of 99.4% (CWRU), 97.8% (PU), and 99.5% (IMS). In addition, its region-aware detection mechanism enables direct visualization of fault locations in spectrograms, offering a practical solution for condition monitoring in rotating machinery.

**Index Terms**—Bearing fault diagnosis, continuous wavelet transform (CWT), time–frequency spectrogram, YOLO object detection.

## I. INTRODUCTION

Rolling bearings are critical components in rotating machinery, and their operational reliability directly influences equipment lifespan, production efficiency, and safety [1]. Studies suggest that nearly 40% of rotating machinery failures originate from bearing faults [2]. These faults are often implicit in dynamic, non-stationary vibration signals, making their early-stage diagnosis particularly challenging. Vibration signals acquired from rotating machinery are typically recorded as one-dimensional time-domain sequences. These raw signals contain temporal patterns related to mechanical faults, such as impulsive features caused by inner race or ball defects [7]. However, these characteristics are often masked by noise and operational variability, especially during early-stage degradation [1]. Moreover, time-domain signals lack explicit frequency information, making it difficult to distinguish fault types that manifest at similar time intervals but differ in spectral behavior [2] (e.g., ball vs. outer race faults, inner race faults vs. imbalance, and looseness vs. misalignment, etc).

Several traditional signal processing methods, such as short-time Fourier transform (STFT), Wigner–Ville distribution (WVD) [3], and Hilbert–Huang transform (HHT) [4], have been widely used to characterize non-stationary signals in

This work was supported in part by the Academia Sinica under Grant 235g Postdoctoral Scholar Program, in part by the NSTC of Taiwan under Grant 113-2926-I-001-502-G. (Corresponding author: *Po-Heng Chou*).

Po-Heng Chou is with the Research Center for Information Technology Innovation (CITI), Academia Sinica (AS), Taipei, 11529, Taiwan (e-mail: d00942015@ntu.edu.tw).

Wei-Lung Mao and Ru-Ping Lin are with the Department of Electrical Engineering, National Yunlin University of Science and Technology (NYUST), Yunlin 64002, Taiwan (e-mail: wlmao@yuntech.edu.tw, anelin21@gmail.com).

both time and frequency domains. However, each of these methods exhibits intrinsic limitations [1], [2]. STFT employs a fixed analysis window, resulting in a fundamental trade-off between time and frequency resolution, which restricts its ability to capture features across multiple scales. WVD offers high resolution in theory, but it suffers from severe cross-term interference when analyzing multi-component signals. This interference often leads to spurious artifacts in the resulting spectrograms, which complicates the interpretation of fault features. HHT is data-adaptive and can decompose signals into intrinsic mode functions (IMFs), but its performance is highly sensitive to noise. Furthermore, it lacks a rigorous mathematical foundation for its empirical mode decomposition (EMD), which undermines the stability and reliability of its instantaneous frequency representation.

In contrast, continuous wavelet transform (CWT) [5], particularly with Morlet wavelets, offers multi-resolution analysis with better localization of both time and frequency content. Its ability to highlight transient features and scale-varying patterns makes it especially effective for capturing early bearing faults [6], which may be subtle and masked by background variations. Therefore, CWT serves as a powerful front-end transformation for fault-related pattern enhancement in complex industrial settings.

While CWT effectively transforms vibration signals into informative two-dimensional time-frequency representations, the subsequent classification stage remains critical. In recent years, deep learning (DL) methods have emerged as powerful tools for bearing fault diagnosis due to their end-to-end learning capability and feature extraction strength [1], [2], [7], [8]. Xia et al. [7] demonstrated early success using CNNs on multi-sensor signals. Pan et al. [8] proposed a hybrid CNN–LSTM model, laying the foundation for Chen et al. [9], who further extended it with multi-scale kernels and stacked LSTMs, and reported over 98% accuracy on bearing datasets.

Despite these achievements, most DL-based models perform global classification on entire signal segments, lacking the spatial interpretability and localization capabilities necessary for fault-aware maintenance. Hakim et al. [10] emphasized this limitation in their systematic taxonomy, highlighting challenges such as interpretability, data dependency, and the need for lightweight architectures suitable for embedded deployment.

To address these limitations, we propose a framework that combines CWT-based time–frequency spectrograms with You Only Look Once (YOLO)-based object detection models, including YOLOv9 [11], YOLOv10 [12], and YOLOv11 [13] to localize and classify fault patterns simultaneously. This approach leverages YOLO’s unified detection pipeline, which is optimized for both accuracy and speed, to enable fast and

spatially explainable bearing fault diagnostics. To the best of our knowledge, this is the first study to explore YOLO-based spatial detection in time–frequency spectrograms for industrial bearing fault applications. The main contributions of this letter are as follows:

- We propose a novel bearing fault diagnosis framework that combines CWT with YOLOv9, v10, and v11 to detect and classify fault patterns directly on time–frequency spectrograms.
- The diagnostic task is reformulated as a spatial object detection problem, enabling region-aware visualization of fault patterns across time and frequency axes.
- The proposed method is validated on three publicly available benchmark datasets, including Case Western Reserve University (CWRU) [14], Paderborn University (PU) [15], and the Intelligent Maintenance Systems (IMS) dataset [16], covering a wide range of operating conditions and fault types, and demonstrating strong generalizability.
- This work is the first unified application of YOLOv9, v10, and v11 for spectrogram-based fault diagnosis, offering a transferable solution that balances high detection accuracy with model compactness and visual interpretability.

## II. SYSTEM OVERVIEW AND PROPOSED CWT-YOLO

The overall architecture of the proposed bearing fault diagnosis system consists of three main stages: (1) time-frequency transformation using CWT, (2) spectrogram pre-processing and labeling, and (3) fault diagnosis using YOLO-based object detectors. Vibration signals acquired from rotating machinery are typically recorded as one-dimensional time-domain sequences. These raw signals contain temporal patterns related to mechanical faults, such as impulsive features caused by inner race or ball defects [7]. However, these characteristics are often masked by noise and operational variability, especially during early-stage degradation [1]. Moreover, time-domain signals lack explicit frequency information, making it difficult to distinguish fault types that manifest at similar time intervals but differ in spectral behavior [2], such as ball vs. outer race defects, early-stage inner race faults vs. imbalance, or looseness vs. misalignment, etc. Fig. 1 illustrates representative examples of such raw vibration signals. While some signal segments contain distinctive fluctuations, they are difficult to interpret visually or distinguish across fault types.

### A. Continuous Wavelet Transform (CWT)

The CWT is a time-frequency analysis tool that decomposes a one-dimensional signal into localized time-scale components using a family of wavelets. Compared to fixed-window methods like the STFT, CWT enables multi-resolution analysis with dynamic windowing, making it especially suitable for analyzing non-stationary signals such as bearing vibrations. The CWT of a signal  $x(t)$  is defined as:

$$\text{CWT}(a, b) = \frac{1}{\sqrt{|a|}} \int_{-\infty}^{\infty} x(t) \psi^* \left( \frac{t-b}{a} \right) dt, \quad (1)$$

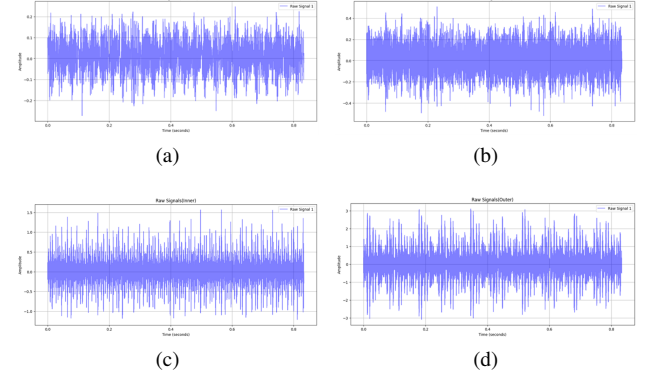


Fig. 1: Sample vibration signals for four bearing conditions: (a) Normal, (b) Ball fault, (c) Inner race fault, (d) Outer race fault. Time (x-axis) and amplitude (y-axis) are shown for illustration.

where  $a$  denotes the scale (inverse frequency),  $b$  is the time shift,  $\psi(t)$  is the mother wavelet, and  $\psi^*(t)$  its complex conjugate.

In this work, we adopt the Morlet wavelet due to its favorable time–frequency localization and robustness to high-frequency noise. The Morlet wavelet combines a sinusoidal carrier with a Gaussian envelope  $\psi(t) = e^{-\frac{t^2}{2}} \cos(5t)$ , which offers balanced resolution across different frequency bands and has shown superior performance in early fault detection [6]. By applying CWT to raw vibration signals, we generate two-dimensional time–frequency spectrograms that expose transient features and scale-dependent energy distributions. These spectrograms serve as spatially structured inputs for subsequent object detection models.

### B. Time–Frequency Spectrogram Visualization

To validate the visual enhancement provided by CWT, we convert the same vibration signals from Fig. 1 into two-dimensional time–frequency spectrograms using Morlet-based wavelet transformation. The resulting images, shown in Fig. 2, capture distinct energy concentration patterns that correspond to different fault types.

Compared to the original one-dimensional signals, these spectrograms exhibit spatially localized frequency bursts that are visually separable. For example, inner race and ball faults typically produce transient, broadband responses, whereas outer race faults show localized energy around characteristic frequencies. These patterns emerge clearly across the time and scale axes after CWT, forming structured visual cues that can be exploited by object detection models. This pre-processing not only standardizes the visual data across datasets but also improves feature discrimination and training stability.

### C. Data Pre-processing and Labeling

To ensure that the CWT-generated spectrograms are suitable for training YOLO-based object detectors, a series of pre-processing and annotation steps are applied to the vibration data prior to model inference.

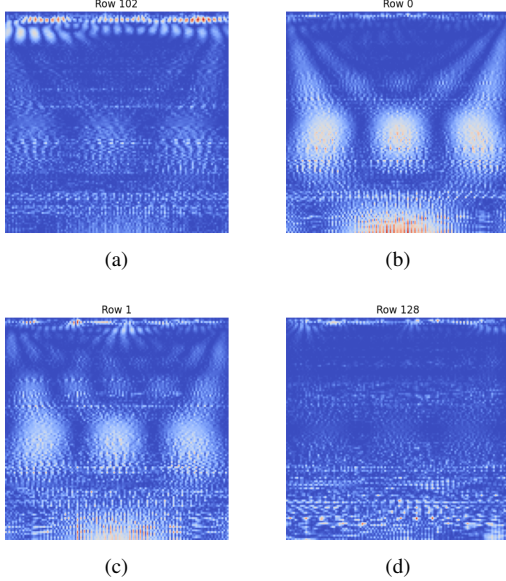


Fig. 2: CWT-based spectrograms for four bearing conditions: (a) Normal, (b) Ball fault, (c) Inner race fault, (d) Outer race fault.

1) *Signal Segmentation and Spectrogram Generation*: For each dataset (CWRU, PU, and IMS), the raw vibration signals are segmented into fixed-length windows, each containing a sufficient number of samples to capture fault-relevant transients. Empirically, a window length of 2048 samples with 50% overlap is used to balance time resolution and data diversity. Each segment is transformed into a 2D time–frequency spectrogram using the Morlet-based CWT described earlier. The resulting grayscale spectrograms are logarithmically compressed and normalized to a  $[0, 1]$  range.

All spectrograms are resized to  $640 \times 640$  pixels to meet the input specification of YOLOv9, v10, and v11 models. This image resolution provides a balance between spatial detail preservation and computational efficiency during training and inference. The resolution of  $640 \times 640$  was empirically selected to balance spectral resolution and GPU memory constraints, while aligning with YOLO model input requirements.

2) *Bounding Box Annotation for Object Detection*: Unlike traditional classification models that produce a single label for an entire signal segment, YOLO models require localized object annotations in the form of bounding boxes. To enable this, we manually annotate each spectrogram using the LabelImg tool, enclosing the time–frequency regions that exhibit fault-specific energy concentrations. Each box is associated with a class label corresponding to one of four fault types: Normal, Ball fault, Inner race fault, and Outer race fault.

These annotations are saved in YOLO format, which specifies each object as a row of normalized values [`class_id`, `x_center`, `y_center`, `width`, `height`] with respect to the image dimensions. For consistency, each dataset is annotated separately to ensure accurate spatial alignment with the visual fault features.

3) *Dataset Splitting and Augmentation*: The labeled dataset is partitioned into training, validation, and test sets using an

80 : 10 : 10 ratio to ensure sufficient coverage and generalization. To further enhance model robustness, we apply data augmentation techniques including horizontal flipping, small-scale rotation  $\pm 5^\circ$ , and contrast jittering. These augmentations simulate minor variations in vibration patterns and imaging conditions that may occur in real-world settings.

Through this pre-processing pipeline, the spectrogram data are transformed into a high-quality object detection dataset with spatially grounded annotations, enabling YOLO models to learn fault-localizing features in both time and frequency domains.

#### D. YOLO-based Fault Detection

In this study, bearing fault diagnosis is formulated as an object detection problem on CWT-generated spectrograms. Rather than assigning a global label to each signal segment, the system identifies and localizes regions of interest (ROIs) where fault-related energy patterns occur, enabling both classification and spatial localization.

We adopt YOLOv9 [11], YOLOv10 [12], and YOLOv11 [13] for their strong detection performance and architectural enhancements tailored to lightweight applications. YOLOv9 introduces programmable gradient information (PGI) and the generalized efficient layer aggregation network (GELAN) backbone for improved gradient flow and multi-scale representation, while removing anchor boxes via an anchor-free detection head. YOLOv10 eliminates the need for non-maximum suppression (NMS) through a dual-label assignment strategy, and uses spatial-channel decoupled downsampling (SCDown) with rank-guided channel interaction block (CIB) blocks to reduce redundancy. YOLOv11 further streamlines the architecture with C3k2 (cross-stage convolutional module with kernel size 2) blocks, the C2PSA (cross-stage partial with spatial attention) attention mechanism, and maintains minimal floating-point operations (FLOPs) and parameter count, making it ideal for embedded deployment.

All models are trained on  $640 \times 640$  spectrograms derived from the CWRU [14], PU [15], and IMS [16] datasets, using bounding box annotations over energy-dense fault regions. A composite loss function including localization, objectness, and classification terms guides the training.

### III. EXPERIMENTAL RESULTS

#### A. Performance Metrics

We evaluate model performance using the following metrics:

- **Mean Average Precision (mAP)**: Computed by averaging the area under the precision-recall curve across all classes and all intersection-over-union (IoU) thresholds. In this study, mAP is reported at an IoU threshold of 0.5 (denoted as mAP@0.5), following standard object detection evaluation protocols.
- **Precision (PRE)**: The proportion of correctly identified positive predictions is calculated by

$$\text{PRE} = \frac{TP}{TP + FP}. \quad (2)$$

TABLE I: Performance (mAP@0.5, Precision, Recall, F1) on CWRU, PU, and IMS.

Dataset	Model	mAP	PRE	REC	F1
CWRU [14]	YOLOv9	99.4%	98.6%	98.5%	98.6%
	YOLOv10	99.4%	99.2%	98.1%	98.6%
	YOLOv11	99.0%	93.9%	98.5%	96.2%
	MCNN-LSTM [9]	96.0%	96.1%	96.1%	96.1%
PU [15]	YOLOv9	91.6%	80.8%	84.8%	82.7%
	YOLOv10	97.2%	89.0%	92.7%	90.8%
	YOLOv11	97.8%	94.9%	93.8%	94.3%
	MCNN-LSTM [9]	77.7%	77.7%	77.4%	77.6%
IMS [16]	YOLOv9	99.5%	99.9%	100.0%	100.0%
	YOLOv10	99.5%	99.9%	100.0%	99.9%
	YOLOv11	99.5%	100.0%	100.0%	100.0%
	MCNN-LSTM [9]	96.8%	96.8%	96.8%	96.8%

- **Recall (REC):** The ability of the model to identify all relevant instances is calculated by

$$\text{REC} = \frac{TP}{TP + FN}. \quad (3)$$

- **F1 Score:** The harmonic mean of precision and recall is calculated by

$$F1 = 2 \cdot \frac{\text{PRE} \cdot \text{REC}}{\text{PRE} + \text{REC}}. \quad (4)$$

Here, TP (true positives) are correctly detected fault regions; FP (false positives) are normal regions misclassified as faults; FN (false negatives) are missed faults.

### B. Experimental Setup

All models are trained and evaluated on three public bearing fault datasets: CWRU [14], PU [15], and IMS [16]. The CWT spectrograms are generated from raw vibration signals with 2048-sample windows and 50% overlap. Images are resized to  $640 \times 640$  pixels and annotated with bounding boxes using the LabelImg tool. The datasets are partitioned into 80% training, 10% validation, and 10% testing splits. All YOLO models are trained for 500 epochs using stochastic gradient descent (SGD) (learning rate=0.01, batch size=8) on a workstation with Intel i7 CPU and RTX 3070Ti GPU.

### C. Performance Comparison Across Datasets

Table I presents the mean average precision (mAP), precision (PRE), recall (REC), and F1 score (F1) for each model on the three datasets. All YOLO variants outperform the baseline MCNN-LSTM model [9] across all metrics and datasets. YOLOv11 consistently delivers the highest performance while also requiring the least inference time. The superior performance of YOLOv11 on the PU dataset is attributed to its spatial-attention mechanism (C2PSA), which effectively highlights localized patterns under varying load conditions. To evaluate the computational efficiency of each model, Table II demonstrates their theoretical FLOPs and parameter counts (Params). Values for the YOLO variants are computed using PyTorch on the same hardware setup described in Section III-B. For MCNN-LSTM, the values correspond to its original compact architecture designed for 1D time-series inputs without spectrogram transformation.

Compared to YOLOv9, YOLOv11 reduces FLOPs by over 97% and parameters by nearly 95%, while achieving

TABLE II: Comparison of model complexity (independent of dataset).

Model	FLOPs (G)	Params (M)
YOLOv9	236.7	48.35
YOLOv10	8.2	2.57
YOLOv11	6.3	2.46
MCNN-LSTM [9]	<b>0.010</b>	<b>0.352</b>

comparable or better accuracy across all datasets. Although MCNN-LSTM remains the most compact model in terms of complexity, its classification accuracy and generalizability are significantly lower. In contrast, YOLOv11 provides a balanced trade-off between efficiency and high detection accuracy, making it suitable for lightweight industrial fault monitoring. The proposed CWT-YOLO framework demonstrates strong generalization across diverse datasets. On the PU dataset, which includes multiple fault types under varying load and speed, YOLOv11 outperforms the baseline by over 16 percentage points in mAP. On the IMS dataset, all YOLO models achieve near-perfect classification, highlighting their ability to capture subtle degradation over long-term operation. Among the YOLO variants, YOLOv11 achieves the best overall performance, combining lower model complexity with faster inference than YOLOv9 and YOLOv10. These results indicate that the spatial detection paradigm, when applied to time-frequency spectrograms, supports accurate and interpretable fault localization.

### IV. CONCLUSION

This letter presents a bearing fault diagnosis framework that combines CWT with YOLO-based object detection to leverage time-frequency spectrograms for localized classification. By converting one-dimensional vibration signals into spatially structured spectrograms, the system enables visual identification of fault patterns using bounding box detection. Evaluations on the CWRU, PU, and IMS datasets confirm that YOLO-based models significantly outperform the MCNN-LSTM baseline in classification accuracy, with YOLOv11 achieving the best balance between detection performance and computational complexity. These results highlight the potential of spectrogram-level object detection for building practical, interpretable, and deployment-ready condition systems.

### REFERENCES

- [1] S. Zhang, S. Zhang, B. Wang, and T. G. Habetler, “Deep Learning Algorithms for Bearing Fault Diagnostics—A Comprehensive Review,” *IEEE Access*, vol. 8, pp. 29857–29881, Feb. 2020.
- [2] D. Neupane and J. Seok, “Bearing Fault Detection and Diagnosis Using Case Western Reserve University Dataset With Deep Learning Approaches: A Review,” *IEEE Access*, vol. 8, pp. 93155–93178, Jun. 2020.
- [3] T. A. C. M. Claesen and W. F. G. Mecklenbrauker, “The Wigner Distribution: A Tool for Time-Frequency Signal Analysis,” *Philips J. Res.*, vol. 35, no. 3, pp. 217–250, 1980.
- [4] N. E. Huang *et al.*, “The Empirical Mode Decomposition and the Hilbert Spectrum for Nonlinear and Non-Stationary Time Series Analysis,” *Proc. Roy. Soc. Lond. A Math. Phys. Eng. Sci.*, vol. 454, no. 1971, pp. 903–995, Mar. 1998.
- [5] H. Li, “Bearing Fault Diagnosis Based on Time Scale Spectrum of Continuous Wavelet Transform,” in *Proc. 2011 8th Int. Conf. Fuzzy Syst. Knowl. Discov. (FSKD)*, Shanghai, China, Jul. 2011, vol. 3, pp. 1934–1937.

- [6] A. R. Patil, S. Buchaiah, and P. Shakya, "Combined VMD-Morlet Wavelet Filter Based Signal De-noising Approach and Its Applications in Bearing Fault Diagnosis," *J. Vib. Eng. Technol.*, vol. 12, pp. 7929–7953, 2024.
- [7] M. Xia, T. Li, L. Xu, L. Liu, and C. W. de Silva, "Fault Diagnosis for Rotating Machinery Using Multiple Sensors and Convolutional Neural Networks," *IEEE/ASME Trans. Mechatronics*, vol. 23, no. 1, pp. 101–110, Feb. 2018.
- [8] H. Pan, X. He, S. Tang, and F. Meng, "An Improved Bearing Fault Diagnosis Method Using One-Dimensional CNN and LSTM," *J. Mech. Eng.*, vol. 64, no. 7–8, pp. 443–452, May 2018.
- [9] X. Chen, B. Zhang, and D. Gao, "Bearing Fault Diagnosis Based on Multi-Scale CNN and LSTM Model," *J. Intell. Manuf.*, vol. 32, no. 4, pp. 971–987, Jun. 2021.
- [10] M. Hakim, A. A. B. Omran, A. N. Ahmed, M. Al-Waily, and A. Abdellatif, "A Systematic Review of Rolling Bearing Fault Diagnoses Based on Deep Learning and Transfer Learning: Taxonomy, Overview, Application, Open Challenges, Weaknesses and Recommendations," *Ain Shams Eng. J.*, vol. 14, no. 4, p. 101945, Apr. 2023.
- [11] C.-Y. Wang, I.-H. Yeh, and H.-Y. M. Liao, "YOLOv9: Learning What You Want to Learn Using Programmable Gradient Information," in *Proc. Eur. Conf. Comput. Vis. (ECCV)*, Cham: Springer, Oct. 2025, pp. 1–21.
- [12] A. Wang, H. Chen, L. Liu, K. Chen, Z. Lin, J. Han, and G. Ding, "YOLOv10: Real-Time End-to-End Object Detection," in *Adv. Neural Inf. Process. Syst. (NeurIPS)*, vol. 37, pp. 107984–108011, Dec. 2024.
- [13] Ultralytics, "YOLOv11: Real-Time Object Detection with Enhanced Feature Extraction," *arXiv preprint arXiv:2501.13400*, Jan. 2025.
- [14] Case Western Reserve University Bearing Data Center, "Bearing Data Center," 2020. [Online]. Available: <https://engineering.case.edu/bearingdatacenter>. Accessed: May 8, 2025.
- [15] C. Lessmeier, J. K. Kimotho, D. Zimmer, and W. Sextro, "Condition Monitoring of Bearing Damage in Electromechanical Drive Systems by Using Motor Current Signals of Electric Motors: A Benchmark Data," in *Proc. Eur. Conf. Progn. Health Manage. Soc.*, Bilbao, Spain, Jul. 2016, pp. 1–8.
- [16] W. Gousseau, J. Antoni, F. Girardin, and J. Griffaton, "Analysis of the Rolling Element Bearing Data Set of the Center for Intelligent Maintenance Systems of the University of Cincinnati," *Surveillance*, Feb. 2018.